J. Mater. Environ. Sci. 4 (2) (2013) 177-192
ISSN : 2028-2508
CODEN: JMESCN

Evaluation of N-containing organic compound as corrosion inhibitor for carbon steel in phosphoric acid

A. Zarrouk [1,*], H. Zarrok [2], R. Salghi [3], B. Hammouti [1], F. Bentiss [4], R. Touir [6], M. Bouachrine [5]

[1]*LCAE-URAC18, Faculté des Sciences, Université Mohammed I[er] B.P. 717, 60000 Oujda, Morocco.*
[2] *Laboratoire des procèdes de séparation, Faculté des Sciences, Université Ibn Tofail BP 242, 14000 Kénitra, Morocco.*
[3] *Equipe de Génie de l'Environnement et de Biotechnologie, ENSA, Université Ibn Zohr, BP 1136 Agadir, Morocco.*
[4]*Laboratoire de Chimie de Coordination et d'Analytique (LCCA), Faculté des Sciences, Université Chouaib Doukkali, B.P. 20, M-24000 El Jadida, Morocco.*
[5] *ESTM, University Moulay Ismail, BP 3130, Toulal, Meknès, Morocco*
[6] *Laboratoire d'électrochimie, corrosion et d'environnement, Faculté des Sciences, Université Ibn Tofail BP 133 Kénitra, Moroc.*

Received 19 Oct 2012, Revised 30 Oct 2012, Accepted 30 Oct 2012
* Corresponding Author. azarrouk@gmail.com.

Abstract
The inhibitor effect of N-1-naphthylethylenediamine dihydrochloride monomethanolate (N-NEDHME) on the corrosion of carbon steel in 2.0 M H_3PO_4 at 303-328Kwas investigated by weight loss, potentiodynamic polarization and electrochemical impedance. The results show that inhibition efficiency increases with the inhibitor concentration, while decreases with temperature. The value of activation energy (E_a), Arrhenius factor, enthalpy and entropy for N-NEDHME values were discussed. Langmuir isotherm was found to provide an accurate description of the adsorption behaviour of the investigated compound. The thermodynamic parameters (adsorption equilibrium constant (K_{ads}), free energy of adsorption (ΔG°_{ads}), adsorption heat (ΔH°_{ads}) and adsorption entropy (ΔS°_{ads})) have been calculated and discussed in detail. Polarization curves show that N-NEDHME acts as a mixed-type inhibitor. The experimental data showed a frequency distribution and therefore a modelling element with frequency dispersion behaviour and a constant phase element (CPE) have been used. Quantum chemical calculation was applied to elucidate the adsorption mode of the inhibitor molecule onto steel surface.

Keywords : Carbon steel; H_3PO_4; Inhibition corrosion; Adsorption; Polarisation curves; EIS.

1. Introduction
Phosphoric acid (H_3PO_4) is widely used in the production of fertilizers and surface treatment of steel such as chemical and electrolytic polishing or etching, chemical coloring, removal of oxide film, phosphating, passivating, and surface cleaning [1]. The use of inhibitors for the control of corrosion for metals and alloys which are in contact with aggressive environment is an accepted practice. Large numbers of organic compounds were studied to investigate their corrosion inhibition potential. All these studies reveal that organic compounds especially those with N, S and O showed significant inhibition efficiency [2-7]. Little work [8-14] appears to have been done on the inhibition of mild steel in phosphoric acid solutions.
DFT (density functional theory) methods have become very popular in the last decade due to their accuracy and less time requirement from the computational point of view [15]. Based on the well-known Hohenberg-Kohn theorems [16], DFT focuses on the electron density, ρ (r), it self as the carrier of all information in the molecular (or atomic) ground state. Important molecular properties of molecules such as E_{HOMO}, E_{LUMO}, ΔEgap, dipole moment, etc., have been correlated with inhibition efficiency of different inhibitors using DFT [17]. In this paper, the kinetics of the corrosion of carbon steel in phosphoric acid have been studied by weight loss, potentiodynamic polarization, electrochemical impedance spectroscopy methods and theoretical studies. The action of N-NEDHME as inhibitor in phosphoric acid medium over a range of acid concentration and solution temperature has also been examined.

2. Experimental details

2.1. Materials

The tested inhibitor, namely, N-1-naphthylethylenediamine dihydrochloride monomethanolate (N-NEDHME) was obtained from Sigma–Aldrich chemical co. and his chemical structure is presented in Fig. 1. The steel used in this study is a carbon steel (Euronorm: C35E carbon steel and US specification: SAE 1035) with a chemical composition (in wt%) of 0.370 % C, 0.230 % Si, 0.680 % Mn, 0.016 % S, 0.077 % Cr, 0.011 % Ti, 0.059 % Ni, 0.009 % Co, 0.160 % Cu and the remainder iron (Fe). The carbon steel samples were pre-treated prior to the experiments by grinding with emery paper SiC (120, 600 and 1200); rinsed with distilled water, degreased in acetone in an ultrasonic bath immersion for 5 min, washed again with bidistilled water and then dried at room temperature before use. The acid solutions (2.0 M H_3PO_4) were prepared by dilution of an analytical reagent grade 85 % H_3PO_4 with double-distilled water. The concentration range of N-NEDHME employed was 10^{-5} M to 10^{-2} M.

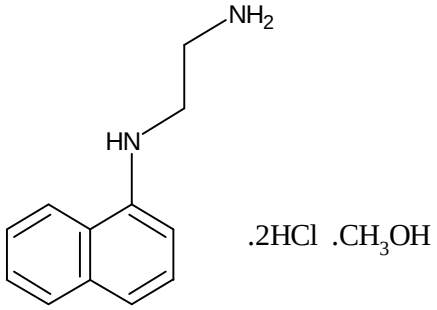

Figure 1. The molecular structure of N-1-naphthylethylenediamine dihydrochloride monomethanolate (N-NEDHME).

2.2. Corrosion tests

2.2.1. Weight loss measurements

The gravimetric measurements were carried out at the definite time interval of 2 h at room temperature using an analytical balance (precision ± 0.1 mg). The carbon steel specimens used have a rectangular form (length = 1.6 cm, width = 1.6 cm, thickness = 0.07 cm). Gravimetric experiments were carried out in a double glass cell equipped with a thermostated cooling condenser containing 50 ml of non-de-aerated test solution. After immersion period, the steel specimens were withdrawn, carefully rinsed with bidistilled water, ultrasonic cleaning in acetone, dried at room temperature and then weighted. Triplicate experiments were performed in each case and the mean value of the weight loss is calculated.

2.2.2. Electrochemical measurements

Electrochemical experiments were conducted using impedance equipment (Tacussel-Radiometer PGZ 100) and controlled with Tacussel corrosion analysis software model Voltamaster 4. A conventional three-electrode cylindrical Pyrex glass cell was used. The temperature is thermostatically controlled. The working electrode was carbon steel with the surface area of 1 cm^2. A saturated calomel electrode (SCE) was used as a reference. All potentials were given with reference to this electrode. The counter electrode was a platinum plate of surface area of 1 cm^2. A saturated calomel electrode (SCE) was used as the reference; a platinum electrode was used as the counter-electrode. All potentials are reported *vs*. SCE. All electrochemical tests have been performed in aerated solutions at 303 K.

For polarisation curves, the working electrode was immersed in test solution during 30 min until a steady state open circuit potential (E_{ocp}) was obtained. The polarization curve was recorded by polarization from -800 to 0 mV/SCE with a scan rate of 1 mV s^{-1}). AC impedance measurements were carried-out in the frequency range of 100 kHz to 10 mHz, with 10 points per decade, at the rest potential, after 30 min of acid immersion, by applying 10 mV ac voltage peak-to-peak. Nyquist plots were made from these experiments. The best semicircle can be fit through the data points in the Nyquist plot using a non-linear least square fit so as to give the intersections with the *x*-axis.

2.3. Quantum chemical calculations

All theoretical calculations were performed using DFT (density functional theory) with the Beck's three parameter exchange functional along with the Lee–Yang–Parr nonlocal correlation functional (B3LYP) [18–20] with 6- 31G* basis set is implemented in Gaussian 03 program package [21]. This approach is shown to yield favorable geometries for a wide variety of systems. This basis set gives good geometry optimizations. The geometry structure of N-NEDHME was optimized under no constraint. The following quantum chemical parameters were calculated from the obtained optimized molecular structure: the energy of the highest occupied molecular orbital (E_{HOMO}), the energy of the lowest unoccupied molecular orbital (E_{LUMO}), the energy band gap ($\Delta E_{gap} = E_{HOMO} - E_{LUMO}$), the dipole moment ($m$) and the total energy (TE).

3. Results and discussion

3.1. Tafel polarization measurement

Fig. 2 shows the potentiodynamic polarization curves for the corrosion of aged maraging steel in 2.0 M phosphoric acid containing different concentrations of N-NEDHME, at 303K. The electrochemical parameters such as corrosion potential (E_{corr}), corrosion current density (i_{corr}) and cathodic Tafel slope (b_c) associated with the polarization measurements for the carbon steel in the presence of different concentrations of N-NEDHME are summarized in Table 1. Since the linear portion of the anodic region is not well defined, the corrosion current densities in all the above cases were determined by the extrapolation of cathodic Tafel slopes to the respective corrosion potentials [22].

The I_{corr} values were used to calculate the inhibition efficiency, $h_{Tafel}(\%)$, (listed in Table 1), using the following equation [23]:

$$h_{Tafel}(\%) = = \frac{I_{corr(uninh)} - I_{corr(inh)}}{I_{corr(uninh)}} \times 100 \quad (1)$$

where $I_{corr(uninh)}$ and $I_{corr(inh)}$ are the corrosion current densities for steel electrode in the uninhibited and inhibited solutions, respectively.

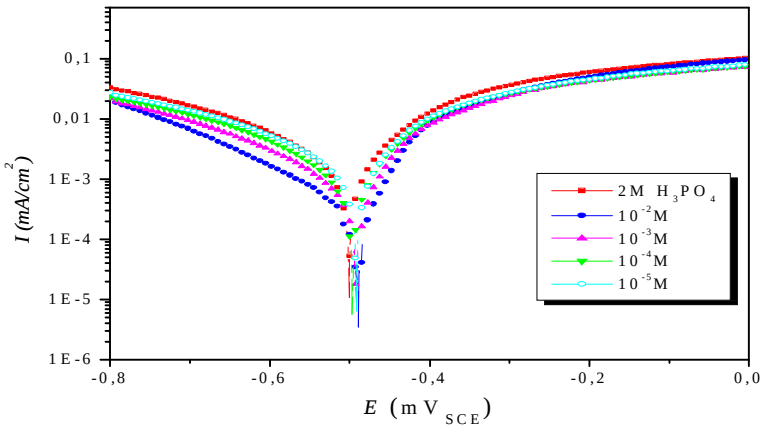

Figure 2. Tafel polarization curves for the corrosion of C38 steel in 2.0 M H_3PO_4 at various concentrations N-NEDHME

The data in the Table 1 clearly show that the N-NEDHME effectively decreases the corrosion current density of the carbon steel, even when added in small concentrations. Inhibition efficiency increases with the increase in the inhibitor concentration up to an optimum value. The maximum quantity of the inhibitor reported in Table 1 corresponds to the optimum concentration of the inhibitor. The presence of inhibitor does not cause any significance shift in the E_{corr} value. This implies that the inhibitor, N-NEDHME, acts as a mixed type inhibitor, affecting both anodic and cathodic reactions [24]. According to Riggs and others [25], if the displacement in corrosion potential is more than ±85 mV/SCE with respect to the corrosion potential of the blank, the inhibitor can be considered as a cathodic or anodic type. But the maximum displacement in the present case is less than 20 mV/SCE, which indicates that N-NEDHME is a mixed type inhibitor. According to Cao [26] if the shift in E_{corr} is negligible, the inhibition is most probably caused by a geometric blocking effect of the adsorbed inhibitive species on the surface of corroding metal.

Table 1. Polarisation parameters and the corresponding inhibition efficiency of carbon steel corrosion in 2.0 M H_3PO_4 containing different concentrations of N-NEDHME at 303 K.

Concentration (M)	E_{corr} vs. SCE (mV)	b_c (mV dec^{-1})	I_{corr} (µA cm^{-2})	h_{Tafel} (%)
Blank	501.9	159.0	2865.7	-
10^{-2}	490.6	160.3	341.1	88.1
10^{-3}	492.8	165.3	758.9	73.5
10^{-4}	497.5	170.7	1148.5	59.9
10^{-5}	492.7	172.4	1423.6	50.3

Fig. 2 indicates that the cathodic polarization curves are parallel and cathodic Tafel slope bc changes only slightly with the increase in the inhibitor concentration. This suggests that the reduction mechanism is not affected by the presence of inhibitor [27,28] and hence the hydrogen evolution is slowed down by the surface blocking effect of the inhibitor. The variation in anodic Tafel slope ba may be due to the adsorption of phosphate ions/or inhibitor molecules on the alloy surface [29]. This indicates that the inhibitive action of N-NEDHME may be considered due to the adsorption and formation of barrier film on the electrode surface. The barrier film formed on the metal surface reduces the probability of both the anodic and cathodic reactions. Thus, the inhibitor, N-NEDHME can be regarded as a mixed type of inhibitor. It is seen from Fig. 2 that at the working electrode potentials, greater than -300 mV/SCE, on the anodic polarization region, the current–potential characteristics do not change in the presence of the inhibitor. Above this potential there is a sharp increase in current density with the increase in the potential, as indicated by the flat region on the anodic curve. This potential can be defined as desorption potential [30]. This phenomenon may be understood by considering the adsorption of the inhibitor molecules on the carbon steel surface and desorption of the inhibitor molecules due to the dissolution of the metal in the corrosion medium; both taking place simultaneously. In this case, the desorption rate of the inhibitor is higher than its adsorption rate, resulting in the increase in the corrosion current with the increase in the potential [31]. At still higher polarization potential the anodic current density change drastically, resulting in sharp increase in Tafel slope.

3.2. Electrochemical impedance spectroscopy

The experimental results obtained from EIS measurements for the corrosion of carbon steel in the absence and presence of inhibitor at 303 K are summarised in Table 2. The impedance spectra for carbon steel in 2.0 M H_3PO_4 without and with various concentrations of N-NEDHME are presented as Nyquist plots in Fig. 3. A considerable increase in the total impedance was recorded with the addition of N-NEDHME, as shown in Fig. 3. It can be concluded from Fig. 3 that the impedance response of carbon steel was significantly changed after the addition of N-NEDHME to the corrosive solutions. This can be attributed to an increase in the substrate impedance with the increase in the inhibitor concentration.

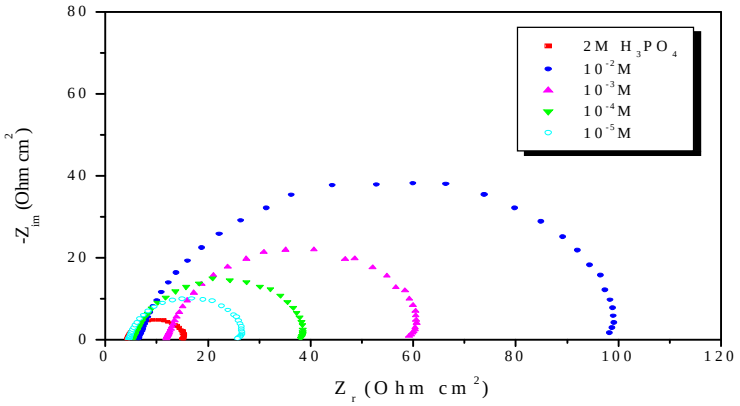

Figure 2. Nyquist plots for carbon steel in 2.0 M H_3PO_4 in the absence and presence of different concentrations of N-NEDHME at 303 K.

It is found that the obtained Nyquist plots are not perfect semicircles due to frequency dispersion and this behaviour can be attributed to roughness and in-homogeneities of the electrode surface [32,33]. When there is

non-ideal frequency response, it is common practice to use distributed circuit elements in an equivalent circuit. The most widely employed is the constant phase element (CPE). In general, a CPE is used in a model in place of a capacitor to compensate for inhomogeneity in the system. Therefore, a constant phase element (CPE) instead of a capacitive element is used to get a more accurate fit of experimental data sets using generally more complicated equivalent circuits. The CPE impedance is given by [34,35]:

$Z_{CPE} = A^{-1} (i\,\omega)^{-n}$ (2)

where A is the CPE constant, ω is the angular frequency (in rad s^{-1}), i^2 =-1 is the imaginary number and n is a CPE exponent which can be used as a gauge of the heterogeneity or roughness of the surface [36]. Depending on the value of n, CPE can represent resistance (n= 0, A = R), capacitance (n=1, A = C), inductance (n = −1, A = L) or Warburg impedance (n = 0.5, A =W).

In this table are shown also the calculated "double layer capacitance" values, C_{dl}, derived from the CPE parameters according to [37]:

$$C_{dl} = (AR_{ct}^{1-n})^{1/n} \quad (3)$$

and the relaxation time constants according to the dielectric theory:

$$t = \frac{1}{2p\, f_{\max}} \quad (4)$$

where f_{max} is the frequency at which appears the maximum in the curve -φ (phase shift) vs. log f. The inhibition efficiency IE (%) is calculated by R_{ct} using Eq. (5), where R^0_{ct} and R_{ct} are the charge-transfer resistance values without and with inhibitor, respectively:

$$IE(\%) = \frac{1/R_{ct}^{\circ} - 1/R_{ct}}{1/R_{ct}^{\circ}} \times 100 \quad (5)$$

The electrical equivalent circuit model shown in Fig. 5 was used to analyze the obtained impedance data. The model consists of the solution resistance (R_s), the charge-transfer resistance of the interfacial corrosion reaction (R_{ct}) and the constant phase angle element (CPE). Excellent fit with this model was obtained with our experimental data. As an example, the Nyquist and Bode plots of both experimental and simulated data of carbon steel in 2.0 M H_3PO_4 solution containing 10^{-2}M of N-NEDHME are shown in Fig. 4. It is clear that the measured impedance plot is in accordance with that calculated by the used equivalent circuit model. The electrochemical parameters, including R_s, R_{ct}, A and n, obtained from fitting the recorded EIS data using the equivalent circuit of Fig. 4, are listed in Table 3.

The inhibition efficiency was evaluated by R_{ct} and C_{dl} values of the impedance. The more densely packed the inhibitor surface film, the larger the diameter of the semicircle, which results in higher R_{ct} and lower C_{dl} values. Results of the present work showed that the R_{ct} values increase with increasing N-NEDHME concentration, while the C_{dl} values tend to decrease (see Table 3). The decrease in C_{dl} values is due to the adsorption of N-NEDHME on the metal surface [38]. This decrease in C_{dl} with increase in N-NEDHME concentration may be explained on the basis that the double layer between the charged metal surface and the solution is considered as an electrical capacitor. The adsorption of N-NEDHME on the electrode surface decreases its electrical capacity because they displace the water molecules and other ions originally adsorbed on the surface.

The decrease in this capacity with increase in N-NEDHME concentration may be attributed to the formation of a protective layer on the electrode surface [29,39]. The thickness of this protective layer increases with increase in inhibitor concentration, since more $N\text{-}NEDHMEH^+$ cations electrostatically adsorb on the electrode surface, resulting in a noticeable decrease in C_{dl} (inspect the C_{dl} values in Table 3). This trend is in accordance with Helmholtz model, given by Eq. (6) [29]:

$$C_{dl} = \frac{\varepsilon_o \varepsilon}{\delta} S \quad (6)$$

where d is the thickness of the protective layer, S is the electrode area, e_o the vacuum permittivity of vide and ε is dielectric constant of the medium.

The inhibiting effectiveness increases with the concentration of the inhibitor to reach a maximum value from 88% to 10^{-2} M.

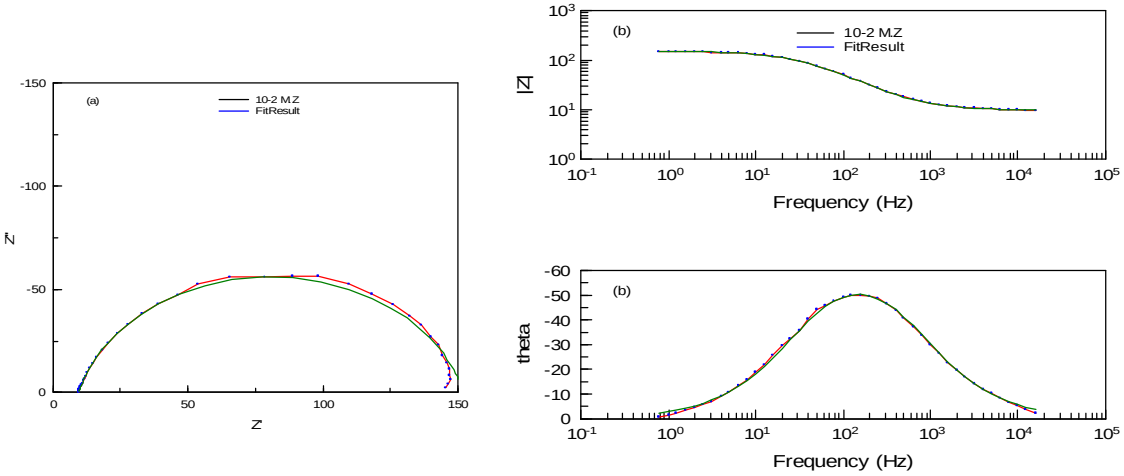

Figure 4. EIS Nyquist (a) and Bode (b) plots for carbon steel/2.0 M H_3PO_4 + 10-2M N-NEDHME interface: (….) experimental data; (—) calculated.

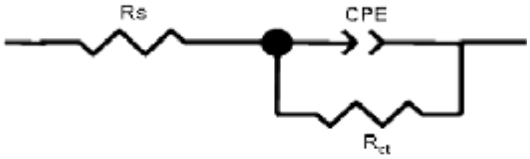

Figure 5. Electrical equivalent circuit used to fit the EIS data of the interface carbon steel/2.0 M H_3PO_4 solution without and with N-NEDHME

Table 3. Impedance parameters and inhibition efficiency values for carbon steel in 2.0 M H_3PO_4 containing different concentrations of N-NEDHME at 303 K.

	Conc (M)	R_s (Ω cm^2)	R_{ct} (Ω cm^2)	n	A×10^{-3}(s^n Ω^{-1}cm^{-2})	C_{dl} (μF cm^{-2})	IE (%)
H_3PO_4	2	4.44	11.46	0.89	0.19103	89.61	-------
N-NEDHME	10^{-2}	6.28	94.64	0.83	0.13780	56.65	87.89
	10^{-3}	9.34	48.67	0.85	0.17371	74.81	76.45
	10^{-4}	5.14	32.57	0.89	0.1456	75.14	64.81
	10^{-5}	4.85	23.48	0.89	0.19358	99.39	51.19

3.3. Gravimetric study

3.3.1. Effect of N-NEDHME concentration

The weight loss of precleaned and dried steel specimens were determined after 2 h of immersion at 303 K by weighing metal samples before and after immersing in 50 cm^3 of 2.0 M H_3PO_4 in absence and presence of various concentration of N-NEDHME. The experiments were performed in triplicate and the average weight loss was recorded. The mean value of corrosion rate and its standard deviations are reported. The corrosion rate (C_R) and inhibition efficiency h_{WL}(%) were calculated according to the Eqs. 7 and 8 [40,41], respectively:

$$C_R = \frac{W_b - W_a}{At} \quad (7)$$

$$h_{WL}(\%) = \left(1 - \frac{w_i}{w_0}\right) \times 100 \quad (8)$$

where W_b and W_a are the specimen weight before and after immersion in the tested solution, w_0 and w_i are the values of corrosion weight losses of carbon steel in uninhibited and inhibited solutions, respectively, A the total area of the carbon steel specimen (cm^2) and t is the exposure time (h).

The inhibition efficiency h_{WL} (%) and corrosion rate (C_R) obtained from weight loss measurements at different concentrations of N-NEDHME in 2.0 M H_3PO_4 solution is shows in Table 4. The inhibition efficiencies increase and the corrosion rate decreases obviously with increasing the concentration of N-NEDHME, which indicates that N-NEDHME has a good performance on inhibition of corrosion for carbon steel in 2.0 M H_3PO_4

solution. The maximum efficiencies reach 88% at the highest concentration. The corrosion inhibition can be attributed to the adsorption of the N-NEDHME at the steel/phosphoric acid solution interface [42]. Indeed, the adsorption of the N-NEDHME could occur due to the formation of links between the d-orbital of iron atoms, involving the displacement of water molecules from the metal surface, and the lone sp2 electron pairs present on the N atoms.

Table 4. Corrosion parameters for carbon steel in aqueous solution of 2.0 M H_3PO_4 in the absence and presence of different concentrations of N-NEDHME from weight loss measurements at 303K.

	Conc (M)	C_R (mg cm^{-2} h^{-1})	h_{WL} (%)	θ
H_3PO_4	2	1.972	---	---
	1×10^{-2}	0.193	90.2	0.902
	5×10^{-3}	0.262	86.7	0.867
N-NEDHME	1×10^{-3}	0.365	81.5	0.815
	5×10^{-4}	0.481	75.6	0.756
	1×10^{-4}	0.666	66.2	0.662
	1×10^{-5}	0.941	52.3	0.523

The variation of C_R and h_{WL}(%) with the N-NEDHME concentration are shown in Fig. 6.

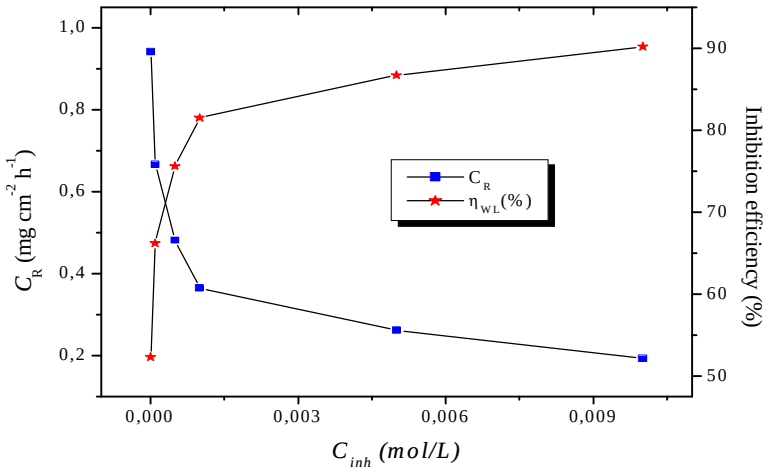

Figure 6. Variation of corrosion rate and inhibition efficiency of carbon steel in 2.0 M H_3PO_4 containing various concentrations of N-NEDHME.

3.1.2. Effect of temperature

The corrosion of a metal in the presence of an inhibitor involves many changes occurring on the metal surface, such as rapid etching and desorption of the inhibitor and the inhibitor itself, in some cases, may undergo decomposition and/or rearrangement [43]. Therefore the effect of temperature on the inhibited acid-metal reaction is highly complex. However, the study of the effect of temperature on the corrosion system facilitates the calculation of many thermodynamic functions for the inhibition and/or the adsorption processes which contribute in determining the type of adsorption of the studied inhibitors.

From Table 5, it can be seen that the inhibition efficiency decreases with the increase in temperature which indicates the probable desorption of inhibitor molecules from the surface of the C-steel as the temperature increases [44]. This is suggestive of physisorption of N-NEDHME molecules on the C-steel surface [45]. But the decrease in inhibition efficiency with the increase in temperature becomes gradual at higher concentrations of the inhibitor.

The activation energy (E_a) for the corrosion process in the presence and absence of the inhibitor, N-NEDHME, were calculated using Arrhenius law Eq. (9) [46]:

$$LnC_R = B - \frac{E_a}{RT} \quad (9)$$

where B is a constant which depends on the metal type and R is the universal gas constant. The plot of Ln C_R versus reciprocal of absolute temperature, 1/T, gives a straight line with slope = - E_a/R, from which the activation energy for the corrosion process can be calculated. The Arrhenius plots for the corrosion of C- steel in the phosphoric acid containing N-NEDHME are shown in Fig. 7.

Table 5 Temperature influence on the weight loss parameters for carbon steel in 2.0 M H_3PO_4 with and without different concentrations of N-NEDHME.

Temperature (K)	Conc (M)	C_R (mg cm^{-2} h^{-1})	h_{WL} (%)	θ
303	Blank	1.972	-----	------
	1×10^{-2}	0.193	90.2	0.902
	5×10^{-3}	0.262	86.7	0.867
	1×10^{-3}	0.365	81.5	0.815
	5×10^{-4}	0.481	75.6	0.756
308	Blank	2.958	-----	------
	1×10^{-2}	0.340	0.885	0.885
	5×10^{-3}	0.534	0.819	0.819
	1×10^{-3}	0.736	0.751	0.751
	5×10^{-4}	0.931	0.685	0.685
318	Blank	5.239	------	------
	1×10^{-2}	0.951	0.818	0.818
	5×10^{-3}	1.629	0.689	0.689
	1×10^{-3}	1.986	0.621	0.621
	5×10^{-4}	2.546	0.514	0.514
328	Blank	9.696	------	------
	1×10^{-2}	2.491	0.743	0.743
	5×10^{-3}	4.133	0.574	0.574
	1×10^{-3}	5.417	0.441	0.441
	5×10^{-4}	6.366	0.343	0.343

The entropy of activation (ΔH_a) and enthalpy of activation (ΔS_a) for the corrosion of alloy were calculated from the transition state theory Eq. (10) [46].

$$C_R = \frac{RT}{Nh}\exp\left(\frac{\Delta S_a}{R}\right)\exp\left(-\frac{\Delta H_a}{RT}\right) \quad (10)$$

where E_a is the apparent activation corrosion energy, R is the universal gas constant, A is the Arrhenius pre-exponential factor, h is Plank's constant, N is Avogrado's number, ΔS_a is the entropy of activation and ΔH_a is the enthalpy of activation.

Fig. 6 shows a plot of Ln (C_R/T) against 1/T. A straight lines are obtained with a slope of ($-\Delta H_a/R$) and an intercept of (Ln R/Nh + $\Delta S_a/R$) from which the values of ΔH_a and ΔS_a are calculated and are listed in Table 6.

Table 6 Activation parameters for the corrosion of carbon steel in 2.0 M H_3PO_4 in the presence of different concentrations of N-NEDHME.

Inhibitor (mM)	E_a (kJ mol^{-1})	ΔH_a (kJ mol^{-1})	ΔS_a (J mol^{-1} K^{-1})	E_a - ΔH_a (kJ mol^{-1})
0.0	51.65	49.03	-77.35	2.62
10.0	84.35	81.73	11.10	2.62
5.0	90.54	87.92	34.57	2.62
1.0	87.63	85.01	27.63	2.62
0.5	84.46	81.84	19.46	2.62

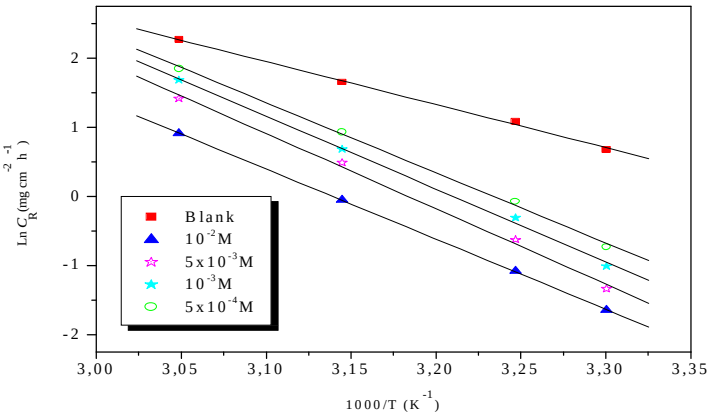

Figure 5. Arrhenius plots for the corrosion of C- steel in 2.0 M H_3PO_4 containing different concentrations of N-NEDHME.

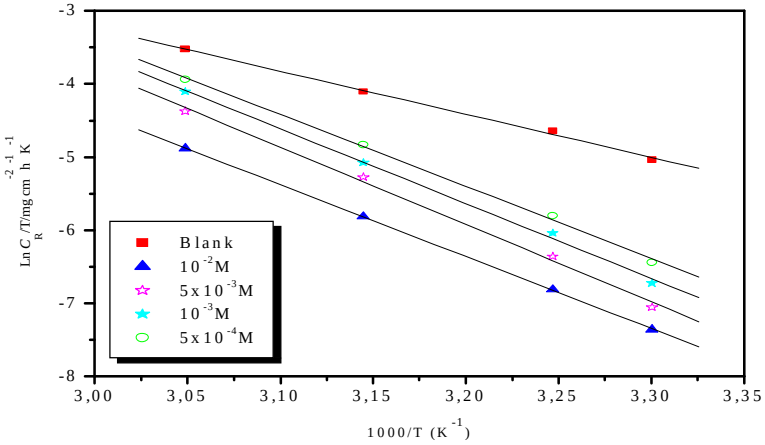

Figure 6. Ln(C_R/T) versus 1/T for the corrosion of C-steel in 2.0 M H_3PO_4 containing different concentrations of N-NEDHME.

The results show that the apparent activation energies at relatively lower concentrations (0–5.0 mM) increase with the concentration of N-NEDHME, while in the range of 5.0–10.0 mM, they decrease with increasing concentrations of N-NEDHME. A similar behaviour has been previously reported in the literature [47,48]. According to Riggs and Hurd [49], the decrease in apparent activation energy at higher levels of inhibition arises from a shift of the net corrosion reaction, from one on the uncovered surface to one directly involving the adsorbed sites. This also reveals that the entire process is surface-reaction controlled, since the energy of activation for the corrosion process, both in the absence and presence of inhibitor, was greater than 20 kJ/mol [50].

Temperature investigations are required, although they do not furnish all of the information needed for the elucidation of adsorption character. There are cases in which chemical adsorption is accepted as the most probable type of adsorption, although h_{WL}(%) decreases with rising temperature and E_a is higher than that in the absence of inhibitor, while physical adsorption is suggested to occur in cases in which the opposite trend is observed [51]. Nevertheless, the adsorption of an organic molecule is not considered as a purely physical or chemical adsorption phenomenon. A wide spectrum of conditions, ranging from the dominance of chemisorptions or electrostatic effects, arises from other experimental data on adsorption [52].

In Table 5, the values of ΔH_a and E_a are nearly the same and are higher in the presence of inhibitor than in a blank solution, indicating that the energy barrier of the corrosion reaction increased in the presence of the inhibitor without changing the mechanism of dissolution [53]. The entropy of activation, ΔS_a, in the absence of the inhibitor is negative, implying that the rate-determining step for the activated complex is the association

rather than the dissociation step, while in the presence of the inhibitor, ΔS_a is positive, which implies that the adsorption process is accompanied by an increase in entropy, which is the driving force for the adsorption of inhibitor onto the C-steel surface [48].
One can notice that E_a and ΔH_a values vary in the same way permitting to verify the known thermodynamic reaction between the E_a and ΔH_a as shown in Table 5 [54]:

$$\Delta H_a = E_a - RT \quad (11)$$

3.1.3. Adsorption considerations

The primary step in the action of inhibitors in acid solutions is adsorption onto the metal surface, which is usually oxide-free. The adsorbed inhibitor then acts to retard the cathodic and/or anodic electrochemical corrosion reaction. It has been reported that the mechanism of inhibition of an inhibitor may vary with factors such as concentration, pH, nature of the anion of the acid, and nature of the metal [55]. Basic information on the interaction between the inhibitor and the carbon steel surface can be provided by the adsorption isotherm. In order to obtain the isotherm, linear relation between θ values (Eq. (11); Table 6) and inhibitor concentration, C_{inh} must be found. Attempts were made to fit the h values to various isotherms including Langmuir, Temkin, Frumkin and Flory-Huggins. By far the best fit is obtained with the Langmuir isotherm. Langmuir adsorption isotherm was found to be the best description of the adsorption behaviour of the studied inhibitor among several adsorption isotherms assessed. Langmuir adsorption isotherm is described by the following equations:

$$\frac{C_{inh}}{q} = \frac{1}{K_{ads}} + C_{inh} \quad (12)$$

where q is the degree of surface coverage and C_{inh} is the inhibitor concentration in the electrolyte and the surface coverage θ is given by

$$q = h_{WL}(\%)/100 \quad (13)$$

where $h_{WL}(\%)$ is the percentage inhibition efficiency as calculated using Eq. (8).
K_{ads} is the equilibrium constant of the adsorption process which is related to the standard Gibbs energy of adsorption, ΔG^{o}_{ads}, according to:

$$K_{ads} = \frac{1}{55.55} \exp\left(\frac{-\Delta G^{o}_{ads}}{RT}\right) \quad (14)$$

where R is the universal gas constant. T the thermodynamic temperature and the value of 55.55 is the concentration of water in the solution in mol/L [56].
Fig. 7 shows the dependence of the fraction of the surface covered C_{inh}/θ as a function of the concentration (C_{inh}) of N-NEDHME.

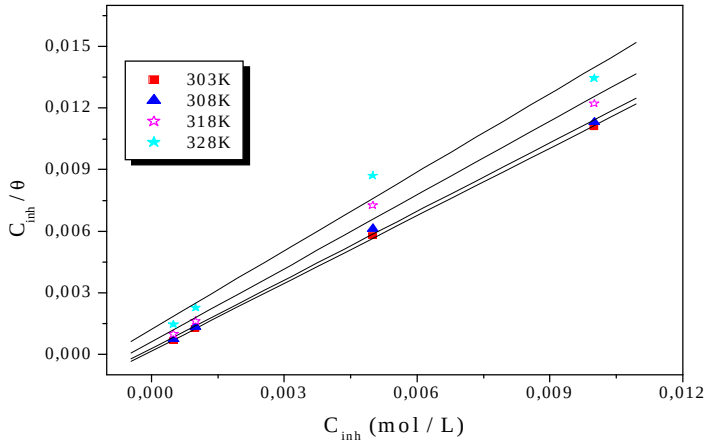

Figure 7. Langmuir adsorption isotherm for the adsorption of N-NEDHME on C-steel surface in 2.0 M H_3PO_4 at different temperatures.

The ΔG^{o}_{ads} values obtained for N-NEDHME on the C-steel surface in 2.0 M H_3PO_4 are between -29 and -32 kJ mol^{-1}. These values indicate that the adsorption process may involve complex interactions involving both physical and chemical adsorption of the inhibitor, as reported by Li et al. [25]. The fact that both ΔG^{o}_{ads} and inhibition efficiency decrease with the increase in temperature, indicates that the adsorption of N-NEDHME on the C-steel surface in phosphoric acid are not favored at high temperature and hence can be considered to be predominantly physisorption. Fig. 8 clearly shows the regular dependence of ΔG^{o}_{ads} on T, indicating a good correlation among thermodynamic parameters.

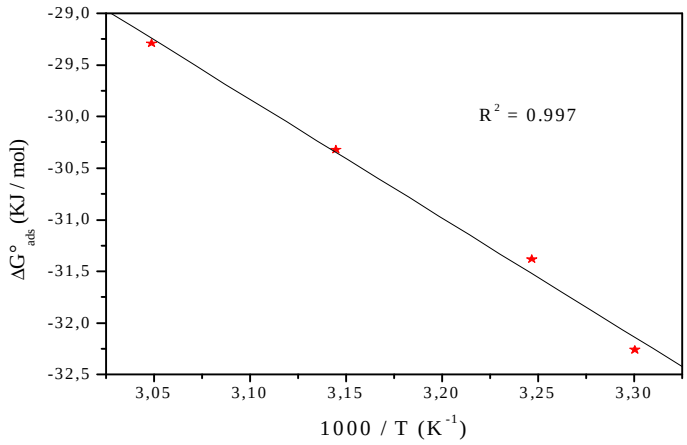

Figure 10. Variation of ΔG^{o}_{ads} versus T on C-steel in 2.0 M H_3PO_4 containing N-NEDHME.

However, physisorption was the major contributor while chemisorptions only slightly contributed to the adsorption mechanism judging from the decrease of h_{WL} (%) with increase in temperature and the higher values of E_a obtained in the presence of inhibitor when compared to its absence.
The enthalpy of adsorption can also be calculated from the Gibbs-Helmholtz equation [57]:

$$\left[\frac{\partial(\Delta G^{\circ}_{ads}/T)}{\partial T}\right]_P = -\frac{\Delta H^{\circ}_{ads}}{T^2} \quad (15)$$

which can be arranged to give the following equation:

$$\frac{\Delta G^{\circ}_{ads}}{T} = \frac{\Delta H^{\circ}_{ads}}{T} + A \quad (16)$$

The variation of ΔG^{o}_{ads}/T with 1/T gives a straight line with a slope which is equal to ΔH^{o}_{ads} (Fig. 9). It can be seen from the figure that ΔG^{o}_{ads}/T decreases with 1/T in a linear fashion. The obtained value of ΔH^{o}_{ads} was – 67.26 kJ mol^{-1}.
Thermodynamically, ΔG^{o}_{ads} is related to the standard enthalpy and entropy of the adsorption process, ΔH^{o}_{ads} and ΔS^{o}_{ads}, respectively, via Eq. (17):

$$\Delta G^{\circ}_{ads} = \Delta H^{\circ}_{ads} - T\Delta S^{\circ}_{ads} \quad (17)$$

and the standard enthalpy of adsorption (ΔH^{o}_{ads}) can be calculated according to the van't Hoff equation [54]:

$$\mathrm{Ln}(K_{ads}) = -\frac{\Delta H^{\circ}_{ads}}{\mathrm{R\,T}} + Const. \quad (18)$$

A plot of Ln (K_{ads}) versus 1000 / T gives a straight line, as shown in Fig. 10. The slope of the straight line is - ΔH^{o}_{ads}/R. The value of ΔH^{o}_{ads} is given in Table 7.

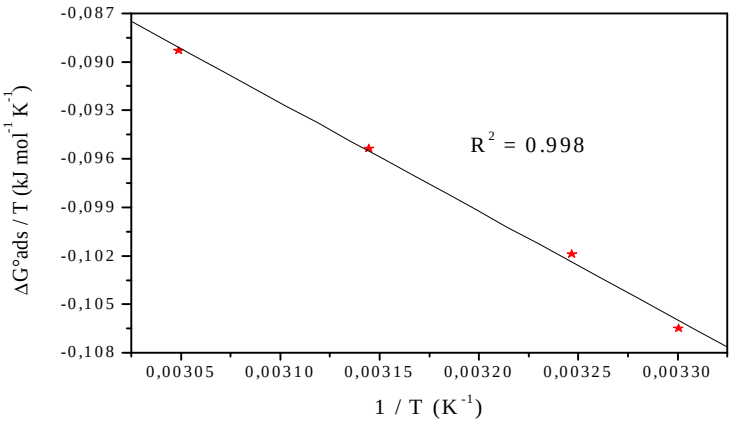

Figure 9. The relationship between ΔG^{o}_{ads} /T and 1/T.

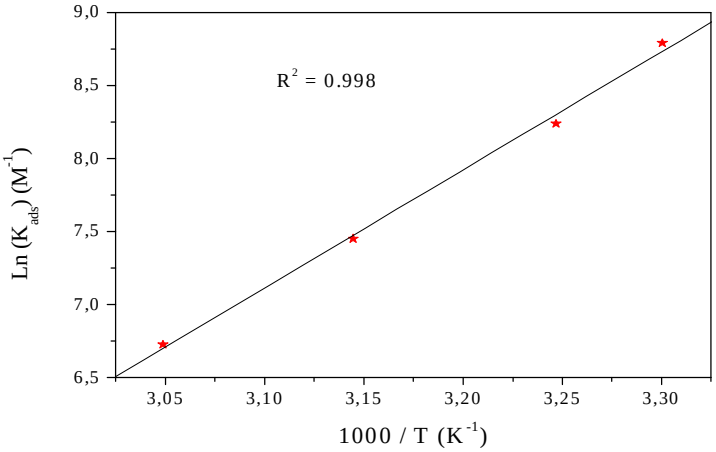

Figure 10. Van't Hoff plot for the C-steel/ N-NEDHME /2.0 M H_3PO_4 system.

The values of thermodynamic parameters for the adsorption of inhibitors are of significant importance in providing a good insight into the mechanism of corrosion inhibition. In general, an endothermic adsorption process ($\Delta H^{o}_{ads} > 0$) is attributed unequivocally to chemisorption [54], an exothermic adsorption process ($\Delta H^{o}_{ads} < 0$) may involve either physisorption or chemisorption or a combination of both the processes. In an exothermic process, the physisorption is distinguished from the chemisorption by considering the absolute values of standard enthalpies of adsorption.

The standard enthalpy of a physisorption process is lower than 40 kJ mol^{-1}, while that of a chemisorption process approaches to 100 kJ mol^{-1} [57]. In the present case, the calculated value of ΔH^{o}_{ads} is -67.29 kJ mol^{-1}, which is an intermediate case [58], probably involving both physisorption and chemisorption.

Table 7 Thermodynamic parameters for the adsorption of inhibitor on metal surface in 2.0 M H_3PO_4.

Temperature (K)	K_{ads} (M^{-1})	R^2	ΔG^{o}_{ads} (kJ mol^{-1})	ΔH^{o}_{ads} (kJ mol^{-1})	ΔS^{o}_{ads} (J mol^{-1} K^{-1})
303	6572.85	0.9998	-32.26		-115.61
308	3783.89	0.9997	-31.38	-67.29	-116.59
318	1720.38	0.9998	-30.32		-116.26
328	833.33	0.9987	-29.29		-115.85

The standard entropy of inhibitor adsorption, ΔS^{o}_{ads}, can be calculated from Eq. (16). The calculated values ΔS^{o}_{ads} are recorded in Table 6. It is obvious that the values of ΔS^{o}_{ads} are negative, as inhibitor molecules move freely in the bulk solution (are chaotic) before adsorption, while as adsorption progresses, the inhibitor molecules adsorbed onto the C-steel surface become more orderly, resulting in a decrease in entropy [59].

3.4. Quantum chemical calculations

Computational methods have a potential application towards the design and development of organic corrosion inhibitors in corrosion field [60]. The studies of Vosta and Eliasek [61] and Chakrabarti [62] can be respected as the first theoretical studies on corrosion inhibitors in the literature. Semi-empirical calculations to evaluate the efficiency of some imidazole derivatives as acidic corrosion inhibitors for steel have been performed by Bereket et al. [63] using AM1, PM3, MNDO and MINDO/3 methods. Recently, the density functional theory (DFT) has been used to analyze the characteristics of the inhibitor/surface mechanism and to describe the structural nature of the inhibitor on the corrosion process [64]. Furthermore, DFT is considered a very useful technique to probe the inhibitor/surface interaction as well as to analyze the experimental data. Thus in the present investigation, quantum chemical calculation using DFT was employed to explain the experimental results obtained in this study and to further give insight into the inhibition action of N-NEDHME on the C-steel surface. Figs. 11-12 show the optimized geometry, the HOMO density distribution and the LUMO density distribution.

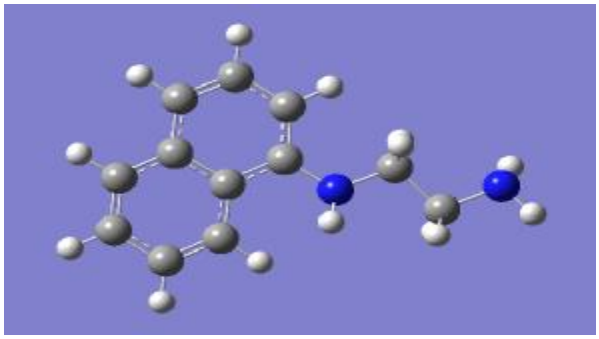

Figure 11. Optimized molecular structure of N-NEDHME by B3LYP-6-31 G(d) method.

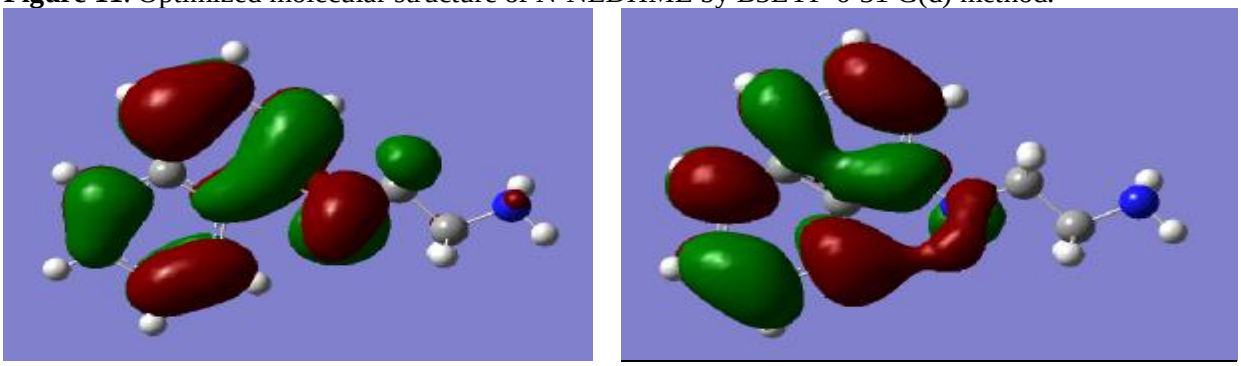

Figure 12. The frontier molecule orbital density distributions of N-NEDHME: HOMO (left); LUMO (right).

Table 8 shows some of the key quantum chemical parameters computed using DFT method. These are mainly the energies of the highest occupied (E_{HOMO}) and lowest unoccupied (E_{LUMO}) molecular orbitals, energy of the gap, ΔE (E_{LUMO} - E_{HOMO}), dipole moment (μ) and total energy (TE). These quantum chemical parameters were obtained after geometric optimization with respect to all nuclear coordinates.

Table 8 The calculated quantum chemical parameters of N-NEDHME.

Compound	TE (u.a)	E_{HOMO} (eV)	E_{LUMO} (eV)	ΔE_{gap} (eV)	μ (Debye)	ΔN
N-NEDHME	-575.20729	- 4.999	- 0.6663	4.332	2.2569	0.96183673

Frontier orbital theory is useful in predicting adsorption centres of the inhibitor molecules responsible for the interaction with surface metal atoms [65]. Moreover, the gap between the LUMO and HOMO energy levels of the molecules was another important factor that should be considered. It has been reported that excellent corrosion inhibitors are usually those organic compounds who are not only offer electrons to unoccupied

orbital of the metal, but also accept free electrons from the metal [66]. It is also well documented in literature that the higher the HOMO energy of the inhibitor, the greater its ability of offering electrons to unoccupied d-orbital of the metal, and the higher the corrosion inhibition efficiency. In addition, the lower the LUMO energy, the easier the acceptance of electrons from metal surface, as the LUMO-HOMO energy gap decreased and the efficiency of inhibitor improved. The calculated molecular properties for N-NEDHME are presented in Table 7. Higher values of E_{HOMO} are likely to indicate a tendency of the molecule to donate electrons to appropriate acceptor molecules with low energy or empty electron orbital. The negative coefficient of E_{HOMO} also confirms the physisorption mechanism [67]. This theoretical result is in agreement with the values of E_a, ΔH^{o}_{ads} and ΔG^{o}_{ads} obtained experimentally. The energy of the LUMO is directly related to the electron affinity and characterizes the susceptibility of the molecule towards attack by neuclophiles. The lower the values of E_{LUMO} are, the stronger the electron accepting abilities of molecules. Low values of the energy gap (ΔE) will provide good inhibition efficiencies, because the excitation energy to remove an electron from the last occupied orbital will be low [68]. A molecule with a low energy gap ismore polarizable and is generally associated with a high chemical reactivity.

According to Pearson [69], when two systems Fe and inhibitors are brought together electrons will flow from lower χ (inhibitor) to higher χ (Fe) until the chemical potentials become equal. As a first approximation, the fraction of electron transferred, ΔN, is given by:

$$\Delta N = \frac{c_{Fe} - c_{inh}}{2\left(h_{Fe} + h_{inh}\right)} \tag{19}$$

where c_{Fe} and c_{inh} denote the absolute electronegativity of iron and the inhibitor molecule, respectively; h_{Fe} and h_{inh} denote the absolute hardness of iron and the inhibitor molecule, respectively. The difference in electro-negativity drives the electron transfer, and the sum of the hardness parameters acts as a resistance [69]. These quantities are related to electron affinity (A) and ionization potential (I) which are useful in their ability to help predict chemical behaviour [70].

$$c = \frac{I + A}{2} \tag{20}$$

$$h = \frac{I - A}{2} \tag{21}$$

I and A are related in turn to E_{HOMO} and E_{LUMO} as follows:

$$I = -E_{HOMO} \tag{22}$$

$$A = -E_{LUMO} \tag{23}$$

Values of χ and η were calculated by using the values of I and A obtained from quantum chemical calculations. Using a theoretical χ value of 7 eV/mol according to pearsons electro-negativity scale [69] and a global hardness η value of 0 eV/mol for Fe by assuming that for a metallic bulk I = A [71], ΔN, which is the fraction of electrons transferred from inhibitor to the mild steel surface was calculated (Table 7). Values of ΔN showed inhibition effect resulted from electrons donation. According to Lukovits [72], if ΔN <3.6, the inhibition efficiency increased with increasing electron donating ability at the metal surface. In this study, N-NEDHME was the donor of electrons, and the C-steel surface was the acceptor. This result supports the assertion that the adsorption of inhibitor on the metal surface can occur on the bases of donor- acceptor interactions between the π-electrons of this compound and the vacant d-orbitals of the metal surface [73].

4. Conclusion

The main conclusions drawn from these studies are weight loss, polarization studies, and impedance measurements which are in reasonably good agreement. The inhibition efficiencies increased with increasing inhibitor concentration but decreased with temperature. E_a for the inhibited solution was higher than that of the uninhibited solution. The adsorption model obeyed the Langmuir adsorption isotherm at all studied temperatures. Thermodynamic adsorption parameters, namely ΔG^{o}_{ads}, ΔH^{o}_{ads} and ΔS^{o}_{ads}, indicated that the adsorption of N-NEDHME molecules was a spontaneous and exothermic process. The variation of inhibition efficiency with temperature and the values of ΔG^{o}_{ads} and ΔH^{o}_{ads} predict both physisorption and chemisorption of this compound on the alloy surface, but predominantly physisorption. Tafel parameters give an idea this inhibitor is mixed-type in nature. Data obtained from ac impedance technique show a frequency distribution

and therefore a modelling element with frequency dispersion behaviour, a constant phase element (CPE) has been used. The calculated corresponding parameters showed increase of the R_{ct} and decrease of the capacitance values with N-NEDHME concentration in the 2.0 M H_3PO_4 medium. The calculated quantum chemical parameters support the good inhibiting performance of this compound.

References

1. Schmitt G., *Brit. Corros. J.*, 19 (1984) 165.
2. Zarrok H., Al-Deyab S. S., Zarrouk A., Salghi R., Hammouti B., Oudda H., Bouachrine M., Bentiss F., *Int. J. Electrochem. Sci*., 7 (2012) 4047.
3. Zarrok H., Oudda H., El Midaoui A., Zarrouk A., Hammouti B., Ebn Touhami M., Attayibat A., Radi S., Touzani R., *Res. Chem. Intermed*. (2012) DOI: 10.1007/s11164-012-0525-x).
4. Zarrok H., Salghi R., Zarrouk A., Hammouti B., Oudda H., Bazzi Lh., Bammou L., Al-Deyab S. S., *Der Pharm. Chem*., 4 (2012) 407.
5. Ghazoui A., Saddik R., Benchat N., Hammouti B., Guenbour M., Zarrouk A., Ramdani M., *Der Pharm. Chem*., 4 (2012) 352.
6. Zarrouk A., Hammouti B., Zarrok H., Salghi R., Dafali A., Bazzi Lh., Bammou L., Al-Deyab S. S., *Der Pharm. Chem*., 4 (2012) 337.
7. Zarrok H., Oudda H., Zarrouk A., Salghi R., Hammouti B., Bouachrine M., *Der Pharm. Chem*. 3 (2011) 576
8. Khamis E., Ameer M.A., Alandis N.M., AL-Senani G., *Corrosion*, 56 (2) (2000) 127.
9. Malki Alaoui L., Hammouti B., Bellaouchou A., Benbachir A., Guenbour A., Kertit S., *Der Pharm. Chem*., 3 (2011) 353.
10. Abu Al-Ola K.A.A., Al-Nami S.Y., *Mod. Appl. Sci*., 5 (2011) 193.
11. Benabdellah M., Touzani R., Dafali A., Hammouti B., El Kadiri S., *Mater. Lett*., 61 (2007) 1197.
12. Benabdellah M., Aouniti A., Dafali A., Hammouti B., Benkaddour M., Yahyi A., Ettouhami A., *Appl. Surf. Sci*., 252 (2006) 8341.
13. Li X., Deng S., Fu H., *Corros. Sci*., 55 (2012) 280.
14. Wang L., Yin G.Y., Zhang Q.F., Pu J.X., *Corrosion*, 56 (2000) 1083.
15. K.F. Khaled, M.A. Amin, Corros. Sci., (2009) 2098.
16. Hohenberg P., Kohn W., *Phys. Rev.*, A136 (1964) 864.
17. Wang H., Wang X., Wang H., Wang L., Liu A., *J. Mol. Model.*, 13 (2007) 147.
18. Becke A.D., *J. Chem. Phys*., 96 (1992) 9489.
19. Becke A.D., *J. Chem. Phys*., 98 (1993) 1372.
20. Lee C., Yang W., Parr R.G., *Phys. Rev. B*., 37 (1988) 785.
21. Gaussian 03, Revision B.01, M. J. Frisch, et al., Gaussian, Inc., Pittsburgh, PA, 2003.
22. McCafferty E., *Corros. Sci*., 47 (2005) 3202.
23. Bouklah M., Benchat N., Aouniti A., Hammouti B., Benkaddour M., Lagrenée M., Vezin H., Bentiss F., *Prog. Org. Coat*., 51 (2004) 118.
24. Jayaperumal D., *Mater. Chem. Phys*., 119 (2010) 478.
25. Li W., He Q., Zhang S., Pei C., Hou B., *J. Appl. Electrochem.*, 38 (2008) 289.
26. Cao C., *Corros. Sci.*, 38 (1996) 2073-2082.
27. Ehteshamzadeh M., Jafari A.H., Naderi E., Hosseini M.G., *Mater. Chem. Phys*., 113 (2009) 986.
28. Ateya B.G., El-Khair M.B.A., Abdel-Hamed I.A., *Corros. Sci.*, 16 (1976) 163.
29. McCafferty E., Hackerman N., *J. Electrochem. Soc*., 119 (1972) 146.
30. Aksut A.A., Lorenz W.J., Mansfeld F., *Corros. Sci*., 22 (1982) 611.
31Amin. M.A., Abd El-Rehim S.S., El-Sherbini E.E.F., Bayoumi R.S., *Electrochim. Acta* ,52 (2007) 3588.
32. Paskossy T., *J. Electroanal. Chem*., 364 (1994) 111.
33. Growcock F.B., Jasinski J.H., *J. Electrochem. Soc*., 136 (1989) 2310.
34. Stoynov Z., *Electrochim. Acta*, 35 (1990) 1493.
35. J.R. Macdonald, *J. Electroanal. Chem.*, 223 (1987) 233.
36. Schultze J.W., Wippermann K., *Electrochim. Acta*, 32 (1987) 823.
37. Martinez S., Metikoš-Hukovic´ M., *J. Appl. Electrochem.*, 33 (2003) 137.
38. Benedetti A.V., Sumodjo P.T.A., Nobe K., Cabot P.L., Proud W.G., *Electrochim. Acta*, 40 (1995) 2657.
39. Bataillon C., Brunet S., *Electrochim. Acta*, 39 (1994) 455.

40. Ahamad I., Prasad R., Quraishi M.A., *Corros. Sci*., 52 (2010) 933.
41. Bentiss F., Outirite M., Traisnel M., Vezin H., Lagrenée M., Hammouti B., Al-Deyab S.S., Jama C., *Int. J. Electrochem. Sci*., 7 (2012) 1699.
42. Wang L., *Corros. Sci*., 48 (2006) 608.
43. Barsoukov E., Macdonald J.R., Impedance Spectroscopy Theory, Experiment, and Applications, second ed., John Wiley & Sons, New Jersey, 2005. pp. 494.
44. Solomon M.M., Umoren S.A., Udosoro I.I., Udoh A.P., *Corros. Sci*., 52 (2010) 1317.
45. Antropov L.I., *Corros. Sci*., 7 (1967) 607.
46. Bentiss F., Lebrini M., Lagrenee M., *Corros. Sci*., 47 (2005) 2915.
47. Noor E.A., Al-Moubaraki A.H., *Mater. Chem. Phys*., 110 (2008) 145.
48. Li X., Deng S., Fu H., Mu G., *Corros. Sci*., 50 (2008) 2635.
49. Riggs O.L. Jr., Hurd R.M., *Corrosion* (NACE) 23 (1967) 252.
50. Fouda A.S., Al-Sarawy A.A., El-Katori E.E., *Desalination*, 201 (2006) 1.
51. Popova A., *Corros. Sci*., 49 (2007) 2144.
52. Moretti G., Guidi F., Grion G., *Corros. Sci*., 46 (2004) 387.
53. Arab S.T., Emran K.M., *Inter. J. App. Chem*., 3 (2007) 69.
54. Zarrouk A., Warad I., Hammouti B., Dafali A., Al-Deyab S.S., Benchat N., *Int. J. Electrochem. Sci*., 5 (2010) 1516.
55. Lece H.D., Emregul K.C., Atakol O., *Corros. Sci*., 50 (2008) 1460.
56. Olivares O., Likhanova N.V., Gomez B., Navarrete J., Llanos-Serrano M.E., Arce E., Hallen J.M., *Appl. Surf. Sci.*, 252 (2006) 2894.
57. Singh A.K., Quraishi M.A., *Corros. Sci*., 52 (2010) 152.
58. Shoesmith D.W., Metals Handbook, ninth ed., vol. 13, ASM International, 1992, p. 18.
59. Mu G., Li X., Liu G., *Corros. Sci*., 47 (2005) 1932.
60. Khaled K.F., *Appl. Surf. Sci*., 255 (2008) 1811.
61. Vosta J., Eliasek J., *Corros. Sci*., 11 (1971) 223.
62. Chakrabarti A., *Br. Corros. J*., 19 (1984) 124-126.
63. Bereket G., Hur H., Ogretir C., J. *Mol. Struct. (THEOCHEM)* 578 (2002) 79.
64. Ebenso E.E., Arslan T., Kandemirli F., Caner N., Love I., *Int. J. Quant. Chem*., 110 (2010) 1003.
65. Fang J., Li J., *J. Mol. Struct. (THEOCHEM)* 593 (2002) 179.
66. Obot I.B., Obi-Egbedi N.O., *Corros. Sci*., 52 (2010) 198.
67. Sahin M., Gece G., Karei E., Bilgic S., *J. Appl. Electrochem*., 38 (2008) 809.
68. Chao P., Liang Q., Li Y., *Appl. Surf. Sci*., 252 (2005) 1596.
69. Pearson R.G., *Inorg. Chem*., 27 (1988) 734.
70. Pearson R.G., Proc. Natl. Acad. Sci. USA 83 (1986) 8440.
71. Dewar M.J.S., Thiel W., *J. Am. Chem. Soc*., 85 (1963) 3533.
72. Lukovits I., Lalman E., Zucchi F., *Corrosion*, 57 (2001) 3.
73. Hackerman N., Snavely Jr. E., Payne Jr. J.S., *J. Appl. Electrochem*., 113 (1966) 677.